Journal of Fluids and Structures (2000) **14,** 323–338
doi:10.1006/jfls.1999.0274 available online at http://www.idealibrary.com on IDEAL®

FLOW-INDUCED MULTIPLE-MODE VIBRATIONS OF GATES WITH SUBMERGED DISCHARGE

P. BILLETER†

Laboratory of Hydraulics (VAW), Swiss Federal Institute of Technology CH-8092 Zurich, Switzerland

AND

T. STAUBLI

Fluidmechanics and Hydromachines, Zentralschweizerisches Technikum Luzern CH-6048 Horw, Switzerland

(Received 10 July 1997, and in final form 18 October 1999)

An experimental investigation of flow-induced vibrations of gates with multiple degrees of freedom is presented. An underflown vertical gate plate with submerged discharge was allowed to oscillate both in the cross-flow (z-) and in the streamwise (x-) direction. The two purposes of the investigation were to further the insight into the hydrodynamic coupling mechanisms of the two vibration modes and to determine the interaction of the unsteady lift and drag forces. Self-excited vibration tests were run with reduced velocities V_{rz} and V_{rx} from 0·8 to 14, covering a range in which the instability-induced excitation (IIE) due to impinging-leading-edge vortices (ILEV) as well as the transition to galloping (MIE) occurred. The ratio of the natural frequencies of the two vibration modes f_{x0}/f_{z0}, the gate opening ratio s/d, and the submergence of the gate plate were varied. Depending on the ranges of reduced velocities and frequency ratios, a complex interaction of two different kinds of instability-induced excitation was detected. Furthermore, it was found that streamwise IIE-excitation and cross-flow galloping coexist. To assess the relevant fluid dynamic amplification and attenuation mechanisms, simultaneous body response and flow velocity measurements were carried out.

1. INTRODUCTION

TYPICAL FEATURES OF FLOW-INDUCED VIBRATIONS of underflown gates are excitation due to instability or lateral deflection of a single shear layer, in contrast to the flow around a bluff body where two shear layers might interact. There is a strong mean-pressure gradient in the streamwise direction. For small gate openings, minor variations of the gate position can dramatically alter both the discharge beneath the gate and the pressure gradient between the head- and the tailwater. Underflown gates with one degree of freedom (d.o.f.) were investigated among many others by Thang (1984, 1990), Thang & Naudascher (1986), Hardwick (1974) and Kolkman (1976), concerning the excitation of cross-flow (vertical) vibrations, and by Jongeling (1988), Thang (1990) and Ishii & Knisely (1989, 1990) with respect to streamwise (horizontal) vibrations. A variety of excitation mechanisms was found [see, e.g., Naudascher & Rockwell (1994)].

For gates with a rectangular gate-lip geometry and flow separation at the leading edge (Figure 1), impinging-leading-edge-vortex excitation (ILEV) and movement-induced

† Current Address: GRUNER Engineering Ltd., CH-4020 Basel, Switzerland.

0889–9746/00/040323 + 16 $35.00/0

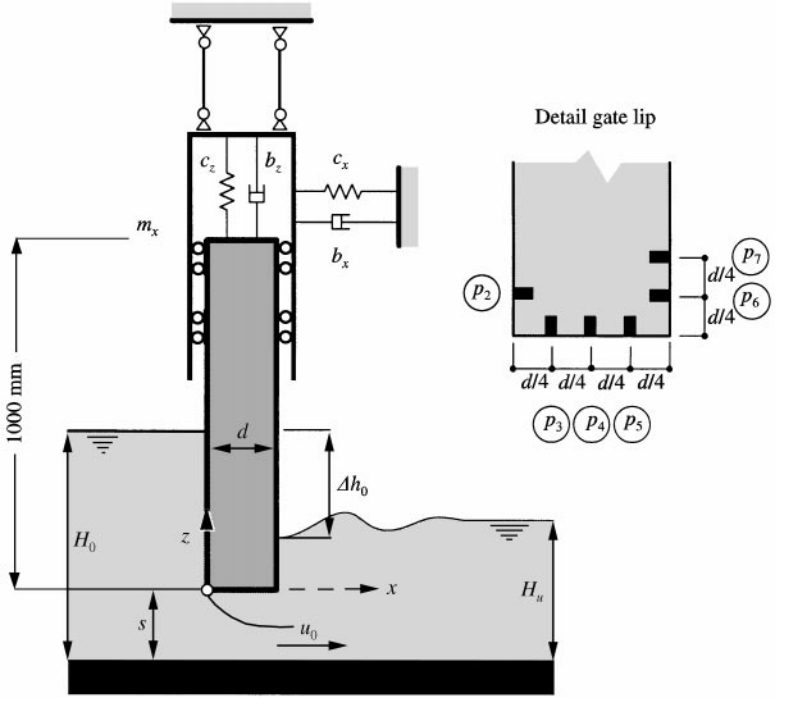

Figure 1. Definition and schematic diagram of the experimental set-up.

excitation (MIE) are the most significant. The ILEV-excitation results from the instability of the efflux shear layer, which is amplified in the presence of the trailing edge of the gate lip. The galloping-type MIE is caused by motion-dependent hydrodynamic mean forces and influenced by discharge and pressure variations (Kanne *et al.* 1991). The ILEV-excitation occurs for small gate openings $s/d \approx 0{\cdot}5$–1 and specific V_{rz} and V_{rx}, respectively. The onset of MIE starts for all $s/d > 0{\cdot}5$, as soon as a critical reduced velocity V_{rz} is exceeded.

Prototype gates, however, must be considered as systems with multiple d.o.f. Most often, there is a variety of bending and torsion modes with typical amplitudes in the streamwise direction. Additionally, there is a mass-oscillation mode in the cross-flow direction for which the whole gate acts as the oscillating mass and the restoring forces are provided by the gate suspensions. The natural frequencies of the bending modes typically lie between 5 and 50 Hz, while the natural frequencies of the mass-oscillation modes range from 2 to 20 Hz. An interaction of several vibration modes is therefore likely to occur (Ishii & Knisely 1992; Billeter 1995). Consequently, the investigation presented aimed subsequently at a better understanding of the hydrodynamic coupling mechanisms between two perpendicular vibration modes.

2. EXPERIMENTAL SET-UP

The test facility consisted of a vertical gate plate of 1 m height which was positioned in a horizontal laboratory flume of about 10 m length and 1 m width (turbulence level of the undisturbed approach flow: Tu $\approx$ 2%). For the vertical direction of motion, the gate plate was guided by linear roller bearings and suspended by coiled springs. The construction itself, providing the vertical d.o.f., acted as a pendulum that was movable in the streamwise

direction and suspended by leaf-springs. Additional damping was supplied by electromagnetic dampers for both directions of motion. The gate behaved as a linear mass oscillator with two perpendicular d.o.f. It was allowed to oscillate in the cross-flow (vertical, z) and the streamwise (horizontal, x) directions (Figure 1). The gate was underflown and had a rectangular bottom lip shape in order to produce maximum fluid dynamic excitation and to exclude any structural coupling. The width of both the gate lip and the gate plate was $d = 10$ cm. The test facility simulated a strip in the mid-section of a weir gate which can be lifted in the vertical direction and is subjected to flexural deflections in the streamwise direction.

The gate lip was equipped with a total of ten miniature pressure transducers which were flush-mounted to the structural surface. The position of the pressure transducers in the mid section of the gate can be seen in Figure 1. The response of the body oscillator was measured by load- and deflection cells which were located at or close to the gate suspensions. The signals of all the gauges were amplified by two carrier-frequency amplifiers and simultaneously digitized (HBM DMC 9012A, with built-in filters). The data were collected by a Macintosh computer using an IEEE-488 interface. The record length was typically 15×2^{12} samples per gauge and the sampling rate was 150 Hz. Applying appropriate FFT-techniques (overlapping Hamming windows, blockwise averaging and both frequency and peak power estimation routines), a frequency resolution of about 0·02 Hz and an amplitude resolution better than 0·2 dB was achieved in the frequency domain.

In order to measure the local flow velocities and to investigate the flow field around the gate lip and in the tailwater of the gate, a Dantec-BSA two-component fibre-optic LDA-system was used. For the assessment of the fluid dynamic excitation mechanism, both simultaneous and synchronized measurements of the body response, the surface pressure and the flow velocity were carried out.

3. ANALYSIS AND PARAMETER VARIATION

Structural coupling between the two d.o.f. can be neglected provided the beams that comprise the pendulum for the horizontal d.o.f. are sufficiently long and of sufficiently small inertia. Upon making this assumption, the equations of motion become

$$\ddot{z} + 2\beta_z \omega_{z0} \dot{z} + \omega_{z0}^2 z = F_{wz}/m_z, \tag{1a}$$

$$\ddot{x} + 2\beta_x \omega_{x0} \dot{x} + \omega_{x0}^2 x = F_{wx}/m_x, \tag{1b}$$

where m_i is the oscillation mass, $\beta_i = b_i/(2m_i\omega_{i0})$ the damping ratio, $\omega_{i0} = 2\pi f_{i0} = (c_i/m_i)^{0\cdot5}$, f_{i0} the natural frequency in air, b_i the viscous damping factor, and c_i the spring rigidity (index i stands for either z or x; Figure 1). For the fluid dynamic excitation forces F_{wi}, which are nonlinear functions $F(x, \dot{x}, z, \dot{z})$, the following linear approach was chosen ($u_0 = (2g\Delta h_0)^{0\cdot5}$ and B is the spanwise width):

$$F_{wz} = \frac{u_0^2}{2} \rho B d C_{Fz} \quad \text{and} \quad F_{wx} = \frac{u_0^2}{2} \rho B d C_{Fx},$$

with

$$C_{Fz} = C_{Fzz} \sin(\omega_z t + \phi_{zz}) + C_{Fzx} \sin(\omega_x t + \phi_{zx}), \tag{2a}$$

$$C_{Fx} = C_{Fxz} \sin(\omega_z t + \phi_{xz}) + C_{Fxx} \sin(\omega_x t + \phi_{xx}), \tag{2b}$$

ϕ_{ij} being the phase shift between deflection and excitation force. Energy is transferred from the flow to the body if $0 < \phi_{ij} < 180^\circ$. All nonlinear components of the self-excited system

are included in the force coefficients C_{Fij} and the phases ϕ_{ij}. C_{Fij} and ϕ_{ij} therefore depend on the geometric, hydraulic and structural parameters. With equation (2), the solution of equation (1) becomes

$$z(t) = z_z \sin(\omega_z t) + z_x \sin(\omega_x t + \varphi_{zx}), \tag{3a}$$

$$x(t) = x_z \sin(\omega_z t - \varphi_{xz}) + x_x \sin(\omega_x t). \tag{3b}$$

Since the amplitudes i_j and the phases φ_{ij} were measured, the force coefficients C_{Fij} and the phases ϕ_{ij} ($\phi_{ij} \neq \varphi_{ij}$) could be determined. A point located on the gate undergoing an oscillation with $z = z_z \sin(\omega_z t)$ and $x = x_z \sin(\omega_z t - \varphi_{xz})$ has an elliptic trajectory. Referring to a coordinate system as shown in Figure 1, the gate acts as a press-shut device if the shorter axis of the ellipse has a positive inclination α, and as a press-open device if the inclination α is negative.

During the investigation, the following parameters were varied: (a) the gate opening s/d, the discharge q underneath the gate and the gate submergence $C_s = (H_o + H_u - 2s)/d$ (the mean velocity u_0 at the *vena contracta* is determined by s/d, q, C_s); (b) the natural frequencies and the damping ratios of the two vibration modes (f_{z0} and f_{x0} were varied between 2·5 and 7·0 Hz).

Self-excited vibration tests were run with reduced velocities $V_{ri} = u_0/(f_i d)$ from 0·8 to 14, covering a range inside which both the ILEV-excitation and the transition to MIE (galloping) occurs (f_i is the vibration frequency). The frequency ratio f_{x0}/f_{z0} ranged between 0·99 and 3·50. With damping ratios β_i between 1·5 and 3%, the Scruton numbers $\mathrm{Sc}_i = 4\pi m_i \beta_i \rho d^2 B$ were between 1·6 and 4·0. The gate opening s/d was varied between 0·5 and 1, and C_s ranged from 1·5 to 6. The Reynolds number $\mathrm{Re} = u_0 d/\nu$ varied between 6×10^4 and 3×10^5.

4. RESULTS

Before discussing selected results of the investigation in detail, some overall features of flow-induced 2-d.o.f. vibrations will be pointed out. Figure 2 shows the power spectra of the vertical suspension force $F_z = z_z c_z$ for different flow velocities u_0. The frequency ratio f_{x0}/f_{z0} is 2·89. It can be seen that with increasing u_0, the dominant vibration amplitudes lie within different frequency ranges. In range A, close to the natural frequency f_{z0} of the vertical d.o.f., dominant vertical vibrations due to ILEV-excitation occur ($2 < V_{rz} < 4$). Range B is linked to the natural frequency f_{x0} of the horizontal d.o.f. and the response of the oscillator becomes much stronger in the horizontal direction ($3{\cdot}5 < V_{rx} < 7$). For high velocities u_0 ($V_{rz} > 10$), the oscillation in the vertical direction is dominant again and the vibration frequencies are within range C which is about $0{\cdot}8 f_{z0}$. These vibrations are caused by MIE as discussed in Section 1. Depending on the reduced velocities V_{rz} and V_{rx}, the system selects an appropriate mode and the properties of these modes will be discussed subsequently. Within ranges A and B, the deflection amplitudes were periodic and nearly harmonic. The influences of both the submergence ratio C_s and of the gate opening s/d will not be considered in this paper. Although they affect quantitatively the vibration phenomena, they do not alter the basic physical properties of the excitation mechanism.

4.1. Dominant Vertical Response, Range A

In Figure 3, the amplitudes z_z/d and x_z/d are plotted versus the reduced velocity V_{rz} for different frequency ratios $f_{x0}/f_{z0} = 1{\cdot}01$ and 1·47 and for the gate with the horizontal d.o.f. blocked ($s/d \approx 0{\cdot}6$). The vertical amplitudes z_z/d are always much stronger than the

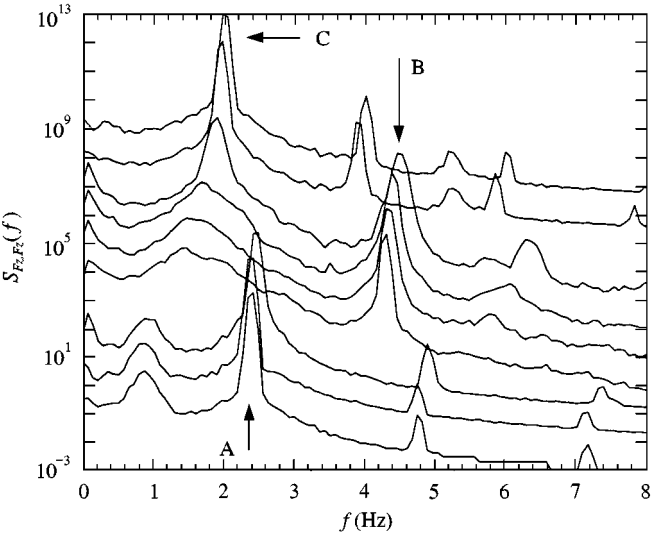

Figure 2. Power spectra of the vertical suspension force F_z. From bottom to top, the flow velocity u_0 is increased. 2-d.o.f., $f_{x0}/f_{z0} = 2{\cdot}89$, $s/d = 0{\cdot}8$–$0{\cdot}9$.

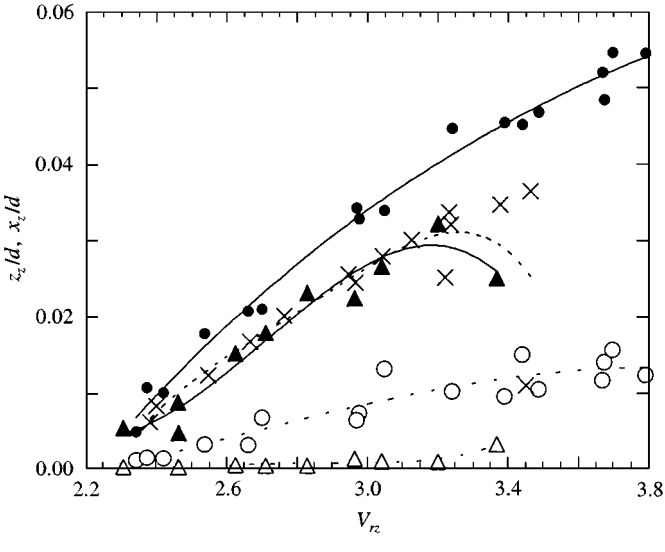

Figure 3. Amplitudes z_z/d and x_z/d: (z: ●, x: ○) 2-d.o.f., $f_{x0}/f_{z0} = 1{\cdot}01$; ($z$: ▲, x: △) 2-d.o.f., $f_{x0}/f_{z0} = 1{\cdot}47$; (×) 1-d.o.f., x-deflection blocked.

horizontal ones (x_z/d). Figure 4 shows the coefficients C_{Fzz} and phases ϕ_{zz} for $f_{x0}/f_{z0} = 1{\cdot}01$ and for the gate with only one z-d.o.f. Typically, the end of the excitation range is associated with a sudden increase of the phase ϕ_{zz}. Comparing the z_z-amplitudes for $f_{x0}/f_{z0} = 1{\cdot}47$ with the data measured for a gate with the horizontal d.o.f. blocked, practically no difference can be found (Figure 3). In principle, this finding also holds for frequency ratios $f_{x0}/f_{z0} > 1{\cdot}5$, although for a frequency ratio $f_{x0}/f_{z0} \approx 2$, the vertical amplitudes might be

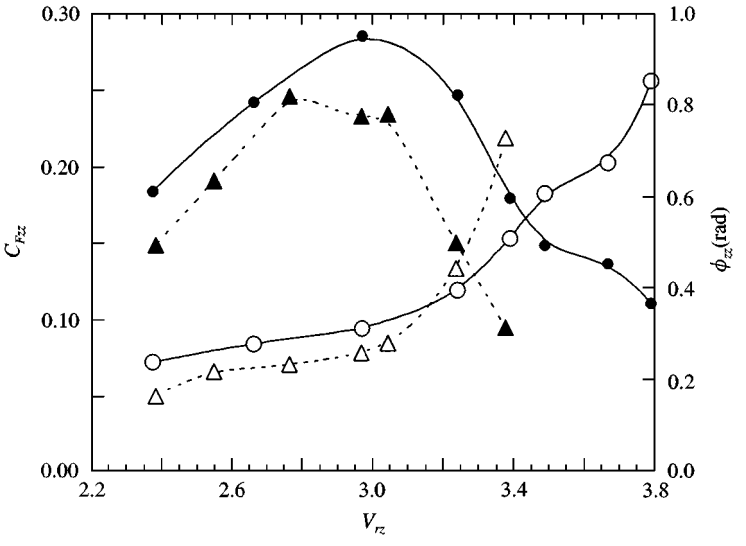

Figure 4. Force coefficient C_{Fzz} and phase ϕ_{zz}: (C_{Fzz}: ●, ϕ_{zz}: ○) 2-d.o.f., $f_{x0}/f_{z0} = 1{\cdot}01$; ($C_{Fzz}$: ▲, ϕ_{zz}: △) 1-d.o.f., x-deflection blocked.

slightly attenuated due to energy transfer from the vertical to the horizontal response (the mechanism is not completely understood, yet). For 1 z-d.o.f. oscillations with comparable Scruton numbers Sc_z and gate openings s/d, both the amplitudes z_z/d and the V_{rz}-range, where the excitation occurs, agree well with the results found by Thang (1984, 1990) and Hardwick (1974). The excitation mechanism is of a vertical ILEV-type (z-ILEV), as will be pointed out later.

If $f_{x0}/f_{z0} \approx 1{\cdot}0$, the vertical amplitudes z_z/d become much larger than the amplitudes of the gate with only one vertical d.o.f., and the range of excitation is extended (Figures 3 and 4). As mentioned before, the trajectory of the gate motion is an ellipse with the longer axis close to both the direction and size of the amplitude z_z/d. Figure 5 shows the angle α_z between the horizontal axis x and the shorter axis of the ellipse. For $f_{x0}/f_{z0} \approx 1$, α_z is smaller than 0 and the gate acts as a press-open device. On the other hand, for $f_{x0}/f_{z0} \geq 1{\cdot}5$, α_z is positive and the gate acts as a press-shut device. Further explanations of the specific behaviour of the vibration orbits will be given in Section 4.3.

4.2. Dominant Horizontal Response, Range B

Streamwise vibrations of gate plates are strongly affected by both added mass and wave effects caused by the headwater and tailwater. The natural frequency of the submerged gate decreases roughly proportionately to $(1/C_s^2)$. Figure 6 shows the horizontal amplitudes x_x/d plotted versus the reduced velocity V_{rx} for three different frequency ratios $f_{x0}/f_{z0} = 1{\cdot}47$, $2{\cdot}07$ and $2{\cdot}46$ as well as for the gate with the vertical d.o.f. blocked ($s/d \approx 0{\cdot}6$). Streamwise vibrations within the range of $1{\cdot}5 < V_{rx} < 2$ were detected as well but will not be considered in this paper. Both the amplitudes x_x/d and excitation range of the gate with one horizontal d.o.f. are in fair agreement with results by Thang (1991) and Jongeling (1988). For the different operation states with 2-d.o.f., the maximum amplitudes x_x/d are not amplified compared to the 1-d.o.f. state. The V_{rx}-range of the maximum excitation, however, is shifted toward smaller V_{rx}. Again, the trajectory of the gate motion is an ellipse, but compared to

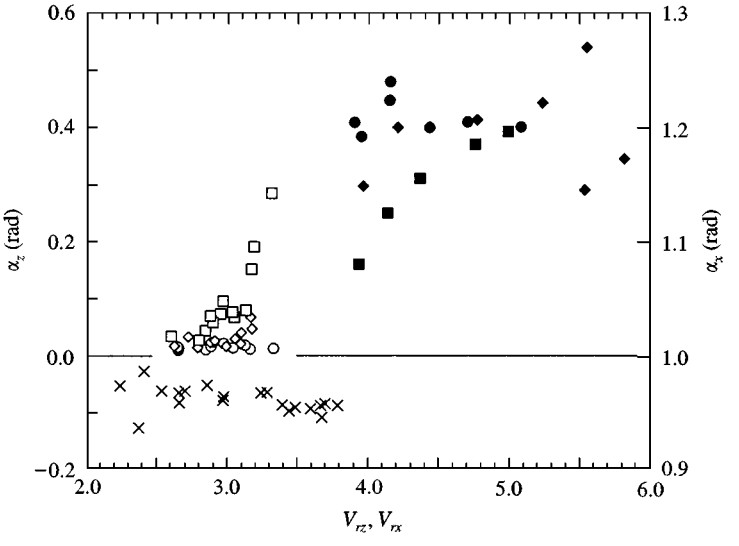

Figure 5. Rotation angle α of the elliptic trajectory: open signs: α_z of dominant $z_z(t)$, solid signs: α_x of dominant $x_x(t)$. (×) $f_{x0}/f_{z0} = 1{\cdot}01$; (□, ■) $f_{x0}/f_{z0} = 1{\cdot}47$; (◇, ◆) $f_{x0}/f_{z0} = 2{\cdot}07$; (●, ○) $f_{x0}/f_{z0} = 2{\cdot}46$.

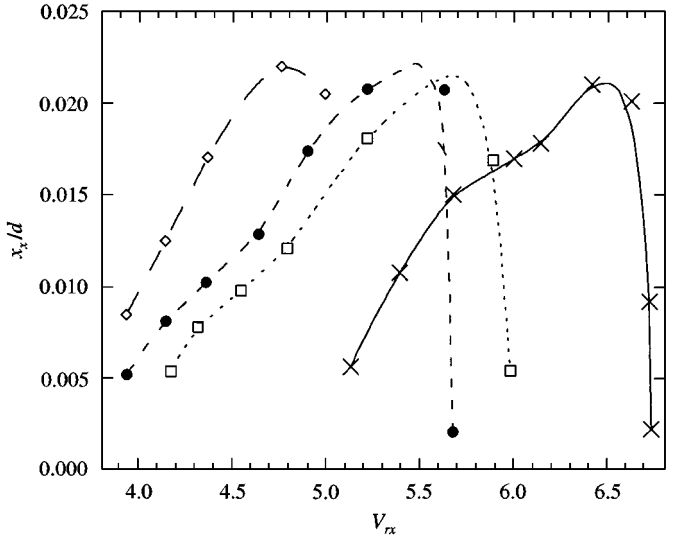

Figure 6. Horizontal amplitudes x_x/d. 1-d.o.f.: (×), no z-deflection. 2-d.o.f.: (□) $f_{x0}/f_{z0} = 2{\cdot}46$; (●) $f_{x0}/f_{z0} = 2{\cdot}07$; (◇) $f_{x0}/f_{z0} = 1{\cdot}47$.

the ILEV-response in the vertical direction, the nondominant amplitude (z_x/d) is much closer to the dominant one (x_x/d). As shown in Figure 5, the angle α_x between the x-axis and the shorter axis of the ellipse is always $\alpha_x > 0$. Thus, the gate behaves as a press-shut device independently of the frequency ratio. The excitation mechanism causing dominant horizontal response will be discussed in the following section.

4.3. Excitation Mechanism

To assess the above-mentioned excitation mechanisms, force, pressure and velocity measurements were carried out at the fixed gate. Using long time-series and averaging techniques in the frequency domain, weak but significant periodic components could be detected in the measured signals. These components emerge from coherent flow structures in the shear layer separating at the leading edge of the gate (the weakly organized vortices are caused by the Kelvin–Helmholtz instability between the separated flow and the jet underneath the gate). Figure 7 shows the power spectra of the gate lift force F_z measured for different flow velocities u_0; (F_z is equivalent to the integrated instantaneous surface pressure). With increasing flow velocities, the location of the weak peaks in the spectra tend towards higher frequencies, suggesting the existence of a convective instabilities with specific Strouhal numbers $\mathrm{Sh}_i = f_i d/u_0$. The data in Figure 7 yields to $\mathrm{Sh}_1 \approx 0{\cdot}4$, $\mathrm{Sh}_2 \approx 0{\cdot}2$, $\mathrm{Sh}_3 \approx 0{\cdot}1$ and accordingly $V_{r1} \approx 2{\cdot}5$, $V_{r2} \approx 5$, $V_{r3} \approx 10$.

In Figure 8, the cross-correlation of simultaneous pressure measurements at the gate and velocity measurements in the tailwater are plotted for increasing streamwise distance between the gate and the location of the velocity measurement. The convection of the persistent flow structure is clearly visible; the convection velocity of these structures amounts to $u_c \approx 0{\cdot}6u_0$. Considering the cross-correlation of 2-D velocity measurements in tailwater (Figure 9), it is observable that with increasing distance from the trailing edge of the gate, flow structures with successively large periods arise. The Strouhal numbers are $\mathrm{Sh}_1 \approx 0{\cdot}36$ and $\mathrm{Sh}_2 \approx 0{\cdot}18$ which is in fair agreement with the Strouhal numbers calculated from the force measurements at the rigid gate. Although the spectral peaks and the maxima of the cross-correlations are rather weak ($R_{ij,\max} \approx 0{\cdot}05$–$0{\cdot}1$), it was concluded that the shear layer has a tendency to form coherent vortical structures; (as a consequence of the great number of blocks used for averging the power spectra and the correlation functions, all peaks are statistically significant; see Section 2). These vortices undergo a vortex pairing process. The pressure variations caused by this process can be detected at the gate itself.

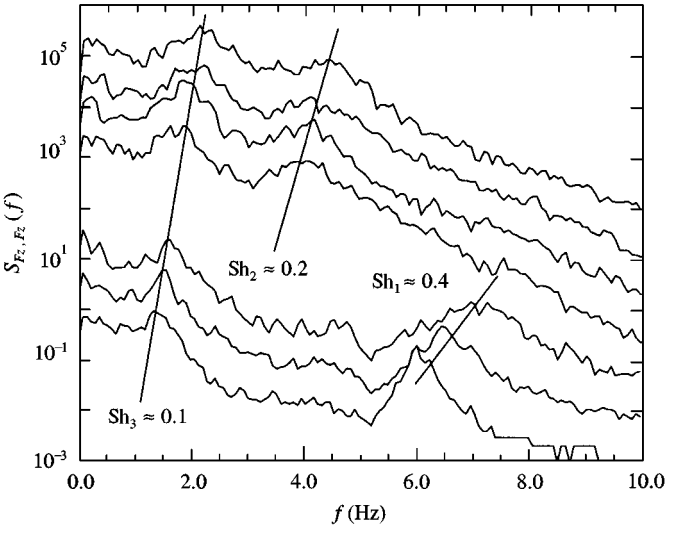

Figure 7. Fixed gate: power spectra of the suspension force F_z. From bottom to top,the velocity u_0 increases from 1·3 to 2·3 m/s.

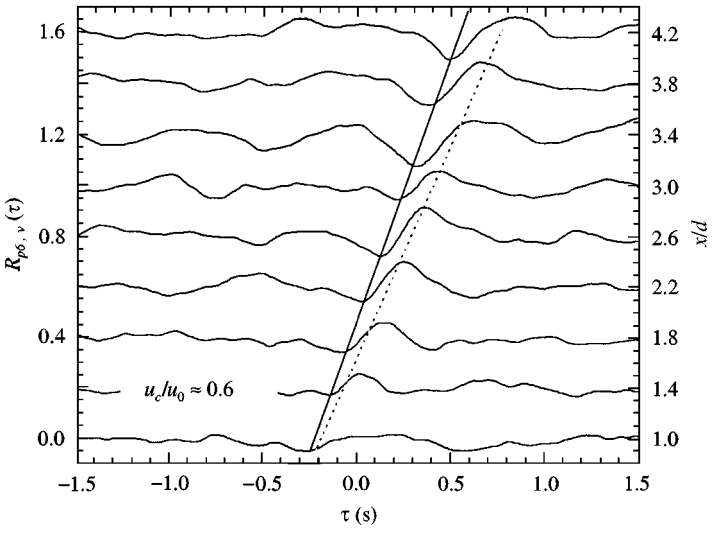

Figure 8. Cross-correlation between cross-flow velocity v' and gate pressure p_6. From bottom to top, the distance x/d between the gate and the velocity measurement is increased (the distance above the channel bed was kept constant at $z/d = -0{\cdot}2$).

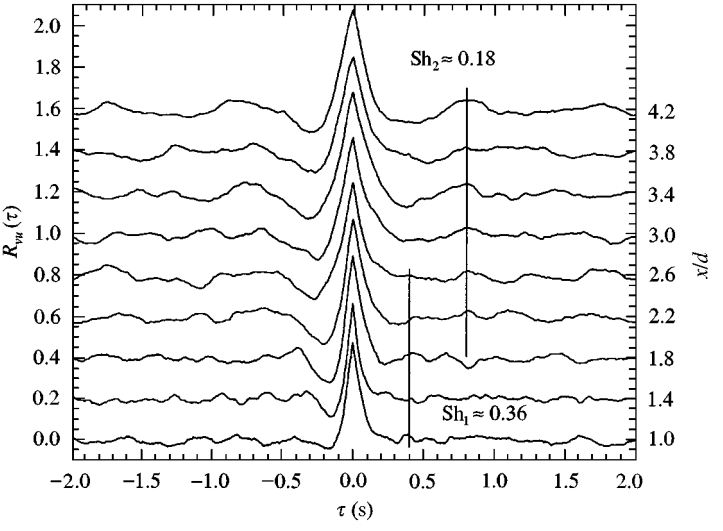

Figure 9. Cross-correlation between the cross-flow and the streamwise velocity (v', u'). From bottom to top, the distance x/d between the gate and the velocity measurement is increased (the distance above the channel bed was kept constant at $z/d = -0{\cdot}2$).

For the further analysis of the excitation mechanisms, the fluctuating pressure coefficients $C'_{pn}(0)$ of the dominant vibration frequencies ω_j were computed from the pressure measurements along the gate lip. Assuming $p_n(t) = p_n \sin(\omega_j t - \varphi_{jn})$, $C'_{pn}(0)$ can be calculated with respect to the gate position $z_j(t) = 0$ or $x_j(t) = 0$ when $\omega_j t = 0, 2\pi, \ldots$:

$$C'_{pn}(0) = \frac{2p_n}{\rho u_0^2} \sin(-\varphi_{jn}), \tag{4}$$

where p_n is the pressure amplitude, and φ_{jn} the phase between deflection and pressure at the respective position (the deflection is either $z_j(t) = z_j \sin(\omega_j t)$ or $x_j(t) = x_j \sin(\omega_j t)$ with $j = z$ or x, depending on the vibration mode to be analysed). A positive $C'_{pn}(0)$ indicates that energy is transferred from the flow to the body and *vice versa*. If the fluctuating pressure is assumed to propagate as a coherent structure along the flow boundary, the convection velocity u_c can be calculated according to

$$u_c = \omega_j \Delta x / \Delta \varphi_{nm}, \tag{5}$$

where ω_j is the circular frequency of the respective vibration mode, $\Delta\varphi_{nm}$ the phase shift between the pressure signals measured at two different positions n, m along the gate lip, and Δx the distance between the two measurement positions n, m.

Subsequently, some properties of the ILEV-excitation causing cross-flow gate vibrations (range A) will be pointed out. The pressure distribution has a wavy shape with growing amplitude towards the trailing edge as was reported previously by Thang (1991) and Hardwick (1974). With increasing V_{rz}, the wave becomes distorted and this results in an increasing instantaneous pressure gradient between the mid-lip position and the trailing edge [Figure 10(a)]. Likewise, at the trailing portion of the gate lip, the relative convection velocity u_c/u_0 of the "pressure wave" (Figure 11) decreases with increasing V_{rz}.

Both of these findings can be considered as intrinsic features of the ILEV-excitation, if we assume that the instability due to the shear-layer impingement is confined between the leading and the trailing edge of the gate. The distortion of the fluctuating pressure distribution and the reduction of the convection velocity are considered to be responsible for the onset of higher harmonics and the nonlinear behaviour of the vibration mechanism

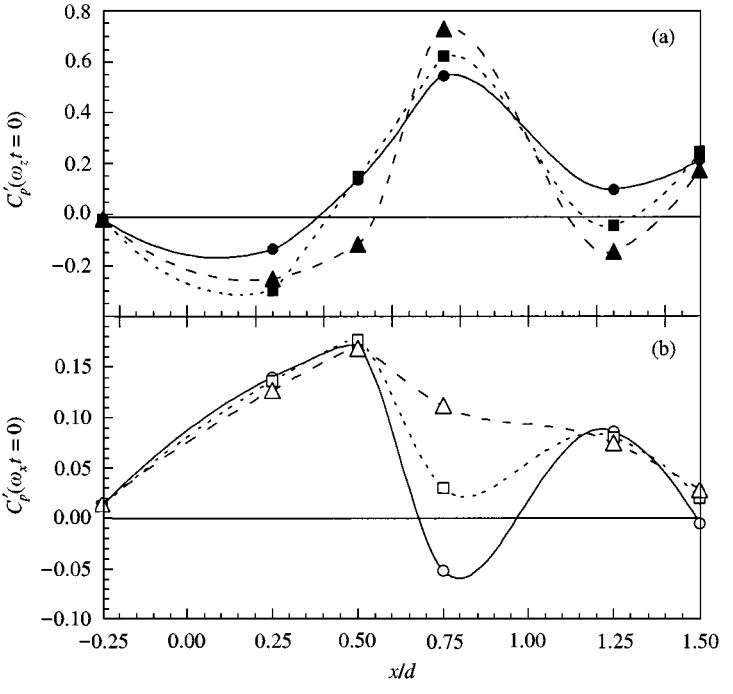

Figure 10. Instantaneous pressure distribution along the gate lip. The pressure measurement points at the vertical faces of the gate are projected on the horizontal axis. (a) Dominant vertical vibration at $\omega_z t = 0$ and $z_z(t) = 0$, $V_{rz} = 2{\cdot}7$ (●), 3·4 (■), 3·8 (▲); (b) dominant horizontal vibration at $\omega_x t = 0$ and $x_x(t) = 0$. $V_{rx} = 3{\cdot}8$ (○), 4·3 (□), 4·6 (△).

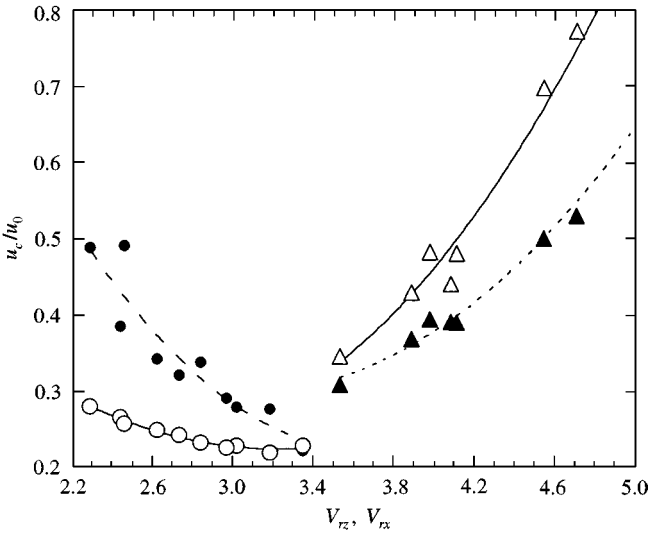

Figure 11. Relative convection velocity of the pressure fluctuations. $z_z(t)$ dominant: (○) $u_c \propto \Delta\varphi(p_3 - p_5)$, (●) $u_c \propto \Delta\varphi(p_4 - p_5)$; $x_x(t)$ dominant: (△) $u_c \propto \Delta\varphi(p_3 - p_5)$, (▲) $u_c \propto \Delta\varphi(p_4 - p_5)$.

towards the end of the excitation range. Supposedly, the abrupt end of the ILEV-excitation range in Figure 3 is associated with the constant convection velocity along the gate lip (Figure 11).

The excitation of streamwise vibration was not completely understood yet. While for vibrations within the range of $1{\cdot}5 < V_{rx} < 2$ a higher mode of ILEV-excitation can be assumed with good reason (Billeter 1998), the excitation between $V_{rx} = 4$ and 8 needs further clarification. According to Thang (1991), the mechanism is a "submode" of ILEV-excitation. Jongeling (1988) gives an explanation that comes close to what Naudascher & Rockwell (1994) refer to as "wake breathing". If we consider the instantaneous pressure distribution along the gate lip [Figure 10(b)], we find that it becomes flattened with increasing V_{rx}. The relative convection velocity u_c/u_0 (Figure 11) increases with increasing V_{rx}, indicating that the vortical structures in the shear layers will be stretched towards the upper end of the vibration range (contrary to the vertical ILEV-excitation for which the vortices are "squeezed"). Taking the findings for the free shear layer beneath the fixed gate into account, as well as the range of reduced velocities V_{rx} where streamwise vibration occur, it can be concluded that a flexible gate (i.e., a flexible locus of flow separation) will enhance and trigger the vortical organization in the shear layer within this distinct range of reduced velocities. Strong interaction of the shear layer and the trailing edge of the gate no longer occurs [compare Figure 10(b) with 10(a) and Figure 12(c,d) with 12(a,b)]. The feedback mechanism, involving the shear-layer instability and its control by the gate motion, will be persistent, as long as the induced pressure fluctuations acting dominantly on the downstream face of the gate [positive $C'_{p6}(0)$ and $C'_{p7}(0)$ in Figures 12(c) and 12(d)] are leading the gate motion. Since the excitation is caused by the motion-induced instability of the shear layer deflecting from the leading edge of the gate, it is suggested that the excitation mechanism should be considered as streamwise body-resonant leading-edge vortex shedding (BR-LEVS). Furthermore, it can be supposed that these findings could apply to other vibration problems involving one single shear layer or two shear layers with symmetrical vortical structures (e.g., streamwise vibrations of short rectangular cylinders in parallel flow).

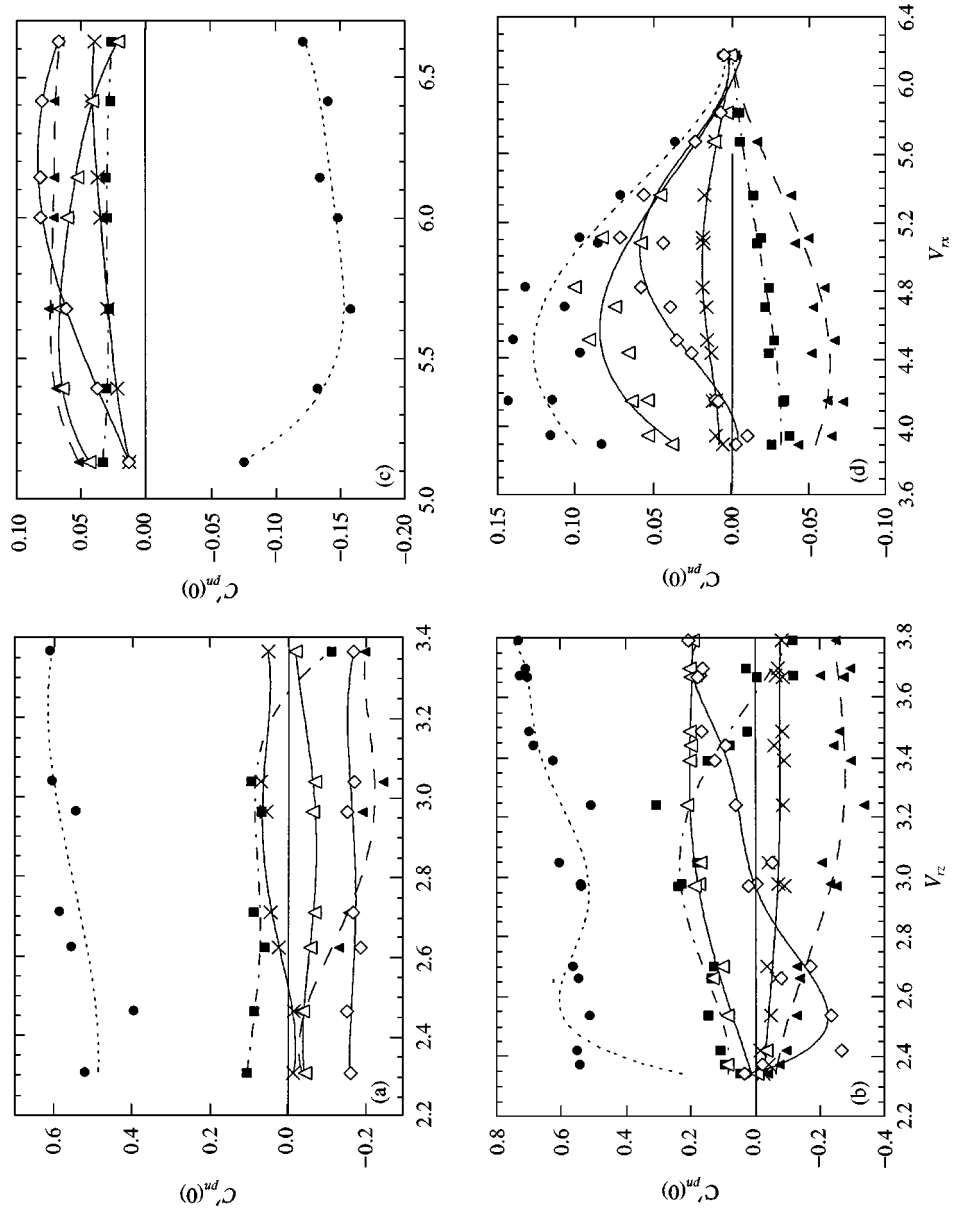

Figure 12. Pressure coefficients $C'_{pn}(0)$ at $z_z(t) = 0$ and $x_x(t) = 0$. $z_z(t)$ dominant: (a) 2-d.o.f., $f_{x0}/f_{z0} = 1{\cdot}47$; (b) 2-d.o.f., $f_{x0}/f_{z0} = 1{\cdot}01$. $x_x(t)$ dominant: (c) 1-d.o.f., $z_z(t)$ blocked; (d) 2-d.o.f., $f_{x0}/f_{z0} = 2{\cdot}5$. ($\times$) $= C'_{p2}(0)$, ($\blacktriangle$) $= C'_{p3}(0)$, ($\blacksquare$) $= C'_{p4}(0)$, ($\bullet$) $= C'_{p5}(0)$, ($\triangle$) $= C'_{p6}(0)$, ($\diamond$) $= C'_{p7}(0)$.

Finally, the coupling between vertical and horizontal vibrations of the gate with 2-d.o.f. are discussed. For this reason, the pressure coefficients as defined in equation (4) are plotted versus the reduced velocities. The $C'_{p3}(0)$, $C'_{p4}(0)$ and $C'_{p5}(0)$ refer to the vertical motion of the gate, while $C'_{p2}(0)$, $C'_{p6}(0)$ and $C'_{p7}(0)$ are related to the streamwise motion (Figure 1). Figure 12(a) shows typical pressure coefficients for an ILEV excitation with $f_{x0}/f_{z0} \geq 1{\cdot}5$. The dominant fluid excitation occurs towards the trailing edge of the gate lip ($C'_{p5}(0)$). The pressure coefficients referring to streamwise excitation are negative, except for $C'_{p2}(0)$ on the upstream face of the gate. Since the phase shift between $x_z(t)$ and $z_z(t)$ is about $\pm\pi$, a high-amplitude $z_z(t)$ motion in the upward direction causes a small-amplitude $x_z(t)$ motion against the streamwise direction. The gate acts as a press-shut device with usually clockwise rotation (at the upper end of the excitation range the rotation may change to counterclockwise). The streamwise vibrations are excited by upstream pressure fluctuations which are caused by discharge variations related to the flow structures travelling along the gate bottom, as suggested by Ishii & Knisely (1989, 1990).

In Figure 12(b), the pressure coefficients for ILEV-excitation and a frequency ratio $f_x/f_z \approx 1$ are shown. The pressure coefficients indicating excitation in the vertical direction behave very similar to the mechanism mentioned above, for up to $V_{rz} \approx 3{\cdot}2$. From $V_{rz} \approx 3{\cdot}2$ to $3{\cdot}8$, $C'_{p5}(0)$ increases further and $C'_{p4}(0)$ decreases below zero. This behaviour can be related to the onset of the streamwise, body-resonant LEVS as pointed out later [Figure 12(d)]. The pressure coefficients indicating streamwise amplification are positive at the tailwater and negative at the headwater face of the gate. Therefore, the amplification of the streamwise motion is caused by the pressure variations from the enhanced shear-layer instability. It can be concluded that for $f_x/f_z \approx 1$, the extension of the vibration range and the increased vibration amplitudes result from the coexistence of vertical ILEV and streamwise, body-resonant LEVS. The x_z-motion is heading the z_z-motion by about $\pi/2$ (see Figure 5) and the gate behaves as a press-open device with counterclockwise rotation.

Figures 12(c) and 12(d) show the pressure coefficients in the range of streamwise vibrations with fixed and released vertical d.o.f. It can be seen that all the pressure coefficients related to streamwise excitation ($C'_{p2}(0)$, $C'_{p6}(0)$ and $C'_{p7}(0)$) are positive. The body-resonant shear-layer instability causes both pressure fluctuations at the trailing portion of the gate and simultaneous pressure alterations in the head water, the latter being produced by discharge variations related to the fluctuating shear layer.

As for the gate with 2-d.o.f., the pressure coefficient representing vertical excitation is reversed compared to the 1-d.o.f. situation. The vertical motion is amplified by the pressure fluctuations caused by the shear-layer instability. These fluctuations affect both the lower portion of the tailwater face of the gate plate and the trailing end of the gate lip. Since the amplitude of $z_x(t)$ is smaller, the amplitude of $x_x(t)$ and $z_x(t)$ lags $x_x(t)$ by a phase angle smaller than π, and the gate will act as a press-shut device again; but, compared to the dominant ILEV-excitation, the rotation is counterclockwise.

4.4. Transition to MIE

Figure 13 shows the vertical vibration amplitudes z_z/d for the gate with 2-d.o.f. and frequency ratios between $f_{x0}/f_{z0} = 2{\cdot}07$ and $3{\cdot}50$ ($s/d \approx 0{\cdot}8$). It seems that neither the onset reduced velocity $V_{rz,\mathrm{crit}}$ nor the vibration amplitudes of the MIE-mechanism are severely affected by the frequency ratio. As shown by Billeter (1998), the basic excitation is caused by galloping, because the pressure coefficients $C'_{p3}(0)$, $C'_{p4}(0)$ and $C'_{p5}(0)$ (pressure along the gate bottom) increase steadily with $z_z\omega_z/u_0$ [the function $\tan^{-1}(z_z\omega_z/u_0)$ is the maximum angle of flow incidence]. The vibration frequency f_z of the MIE-mechanism is only about $0{\cdot}8\, f_{z0}$ (Figure 2, range C). For the small gate openings investigated ($0{\cdot}5 < s/d < 1$), the

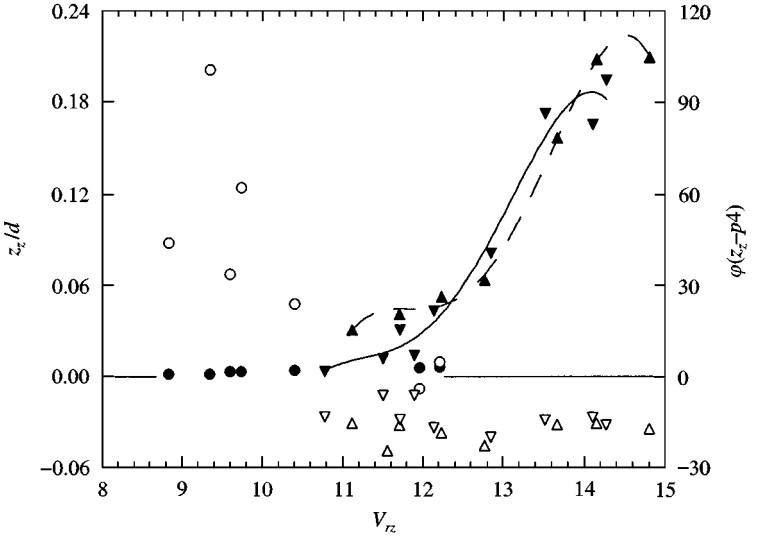

Figure 13. Transition to vertical MIE with simultaneous horizontal LEVS-excitation: vibration amplitudes z_z/d (solid signs) and phases $\varphi(z_z - p_4)$ (open signs); (●, ○) $f_{x0}/f_{z0} \approx 2{\cdot}07$, (▼, ▽) $f_{x0}/f_{z0} \approx 2{\cdot}89$, (▲, △) $f_{x0}/f_{z0} \approx 3{\cdot}50$.

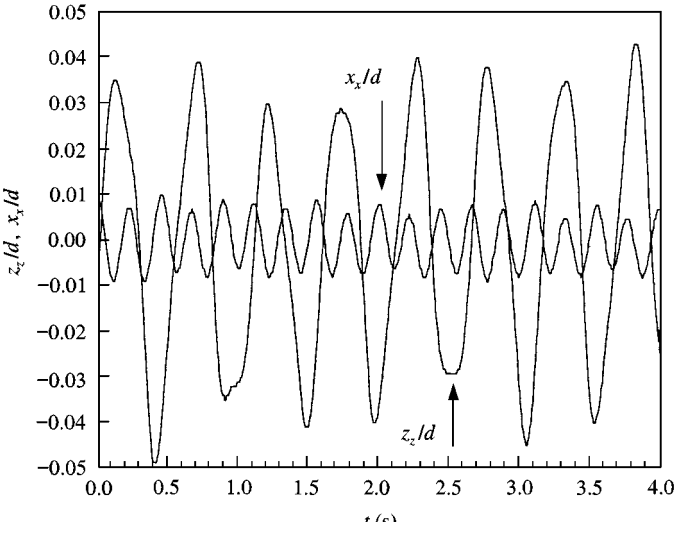

Figure 14. Transition to MIE, time series of vertical and horizontal amplitudes $z_z(t)$ and $x_x(t)$, $V_{rz} = 13{\cdot}0$, $f_{x0}/f_{z0} = 2{\cdot}89$.

hydrodynamic mean lift coefficient is negative and almost proportional to the gate opening (Thang & Naudascher 1986). Since the instantaneous gate opening is in-phase with the gate deflection, the mean lift force is in-phase with the gate deflection, and it thus acts as negative rigidity with regard to the vertical vibration. Consequently, the vibration frequency f_z drops below f_{z0}.

If the reduced velocities of both the horizontal and vertical modes happen to lie within their excitation range, simultaneous vertical and horizontal vibrations $z_z(t)$ and $x_x(t)$ at different frequencies can occur (Figure 14). As long as the vibration frequencies f_x and f_z are

incommensurate, both the horizontal and the vertical vibration modes are caused by independent excitation mechanisms (i.e., cross-flow MIE and streamwise body-resonant LEVS). Especially, the vertical vibration then behaves strongly nonlinearly with modulations in the amplitude and the frequency.

Since the natural frequency of the vertical mode is most often smaller than the frequency of the horizontal one for prototype gates, it was investigated whether vertical vibrations associated with MIE could be excited by subharmonic modes of simultaneously occurring horizontal vibrations. Figure 13 also shows the phases φ_{z4} between the vertical amplitude $z_z(t)$ and the pressure p_4 acting on the gate lip bottom. Negative phases φ_{z4} refer to energy transfer from the flow to the body (the phase φ_{jn} is defined as $p_n(t) = p_n \sin(\omega_j t - \varphi_{jn})$. For the $\frac{1}{2}$-subharmonic mode of a horizontal vibration, lying between $8 < V_{rz} < 11$, the phases are always positive. It can be concluded, therefore, that the MIE is not amplified by $\frac{1}{2}$-subharmonic of the horizontal vibration. The onset of MIE occurs at $V_{rz,\mathrm{crit}} \approx 11$, as soon as the horizontal and the vertical vibration frequencies become incommensurate ($f_x/f_z > 2$).

5. CONCLUSIONS

It was shown that flow-induced vibrations of gates with two degrees of freedom (d.o.f.) are caused by three dominant excitation mechanisms: cross-flow and streamwise ILEV-excitation (z- and x-ILEV), streamwise body-resonant LEVS (x-BR-LEVS) and cross-flow MIE (z-MIE). Characteristic properties of the different excitation mechanisms were pointed out. Depending on the frequency ratio of the two vibration modes and the type of excitation involved, the mutual interaction of the two modes can affect both the vibration trajectory (i.e., the size and the phase angle of the amplitudes) as well as the excitation range.

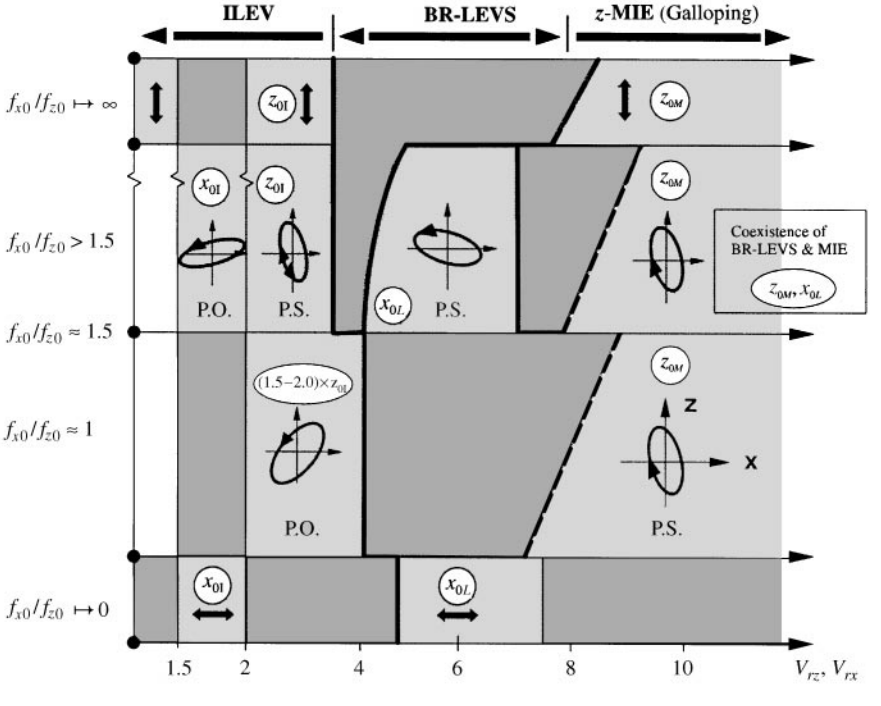

Figure 15. Characteristic vibration trajectories of underflown gates with one or two d.o.f. plotted as a function of the reduced velocities V_{rz} and V_{rx}, respectively, and the frequency ratio f_{x0}/f_{z0}.

A summary of these findings is given in Figure 15: the characteristic flow-induced vibration trajectories of underflown gates with one or two d.o.f. are shown as a function of the reduced velocities V_{rz} and V_{rx}, respectively, and the frequency ratio f_{x0}/f_{z0} ($f_{x0}/f_{z0} = 0$: 1-d.o.f. in x-direction, z-deflection blocked; $f_{x0}/f_{z0} \rightarrow \infty$: 1-d.o.f. in the z-direction, x-deflection blocked). For every vibration trajectory of the gate with 2-d.o.f., the maximum amplitude of the dominant vibration mode is related to the reference amplitude of the respective 1-d.o.f. gate vibration mode within the same excitation range; (reference amplitudes of a gate with 1-d.o.f.: x_{0I} is the maximum x-amplitude for x-ILEV excitation, z_{0I} the maximum z-amplitude for z-ILEV exciation, x_{0L} the maximum x-amplitude for x-BR-LEVS excitation, and z_{0M} the maximum x-amplitude for z-MIE excitation). Furthermore, it is indicated whether the gate acts as a press-shut (PS) or a press-open device (PO).

As shown in Figure 15, the existence of a second d.o.f. rather effects the excitation range and the vibration trajectory than the size of the maximum vibration amplitude. For a frequency ratio close to one, however, cross-flow ILEV and streamwise LEVS-excitation coexist due to fluid dynamic coupling. Compared to gates with only 1 d.o.f., this mechanism extends both the excitation range and the vibration amplitudes. More detailed results and an extended analysis of the findings of the study presented here can be found in Billeter (1998).

ACKNOWLEDGEMENT

Financial support, provided by the Swiss Federal Institute of Technology (ETHZ) and the Laboratory of Hydraulics (VAW), is gratefully acknowledged.

References

Billeter, P. 1995 Flow-induced multiple-mode vibrations of a prototype weir gate. *Proceedings XXVI IAHR Congress*, Vol. 1C, pp. 421–426, London, U.K.

Billeter, P. 1998 Stömungsinduzierte Schwingungen von Schützen mit mehreren Freiheitsgraden. *VAW Mitteilung* **125,** Versuchsanstalt für Wasserbau, Hydrololgie und Glaziologie der ETH Zürich, Zürich (in German).

Hardwick, J. D. 1974 Flow-induced vibrations of vertical-lift gate. *ASCE Journal of Hydrautics Division* **100,** 631–644.

Ishii, N. & Knisely, C. W. 1992 Flow-induced vibration of shell-type long-span gates. *Journal of Fluids and Structures* **6,** 681–703.

Ishii, N. & Knisely, C. W. 1990 Shear layer behaviour under a streamwise vibrating gate and its significance to gate vibration. *JSME International Journal* (Series III) **33,** 131–138.

Ishii, N. & Knisely, C. W. 1989 Shear layer dynamics and unsteady discharge beneath a long span gate undergoing streamwise vibrations. *Proceedings Hydrocomp*, pp. 500–509. Dubrovnik: Elsevier.

Jongeling, T. H. G. 1988 Flow-induced self-excited in-flow vibrations of gate plates. *Journal of Fluids and Structures* **2,** 541–566.

Kanne, S., Naudascher, E. & Wang, Y. 1991 On the mechanism of self-excited vertical vibration of underflow gates. *Proceedings International Conference on Flow-Induced Vibration*, pp. 405–410, Brighton. London: IMechE, Vol. 1991-6.

Kolkman, P. A. 1976 Flow-induced gate vibrations. *Delft Hydraulics Laboratory Publication*, No. 164.

Naudascher, E. & Rockwell, D. 1994 *Flow-Induced Vibrations — An Engineering Guide*; IAHR Hydraulic Structures Design Manual Rotterdam: A.A. Balkema.

Thang, N. D. 1990 Gate vibrations due to unstable flow separation. *ASCE Journal of Hydrautic Engineering* **116,** 342–361.

Thang, N. D. 1984 Strömungsbedingte Schwingungen unterströmter Schützen. *Forschungsberichte VDI*, Reihe 4, No. 66, Düsseldorf (in German).

Thang, N. D. & Naudascher, E. 1986 Self-excited vibrations of vertical lift gates. IAHR *Journal of Hydrautic Research* **24,** 391–404.